Micro and Nanostructures 189 (2024) 207812

Contents lists available at ScienceDirect

Micro and Nanostructures

journal homepage: www.journals.elsevier.com/micro-and-nanostructures

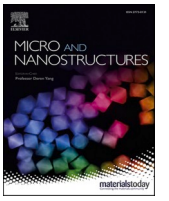

CGS/CIGS single and triple-junction thin film solar cell: Optimization of CGS/CIGS solar cell at current matching point

Rafik Zouache [a], Idris Bouchama [b,c], Okba Saidani [a], Mohamed Amine Ghebouli [c], M. Saeed Akhtar [d], M.A. Saeed [d], Samah Boudour [e,*], Leila Lamiri [e], Ouafia Belgherbi [e], Meriem Messaoudi [e]

[a] ETA Laboratory, Department of electronics, Faculty of technology, University of Mohamed El Bachir El Ibrahimi, Bordj Bou Arréridj, 34000, Algeria
[b] Electronics Department, Faculty of Technology, University of Msila, Msila, 28000, Algeria
[c] Research Unit on Emerging Materials (RUEM), University of Ferhat Abbas, Setif1, 19000, Algeria
[d] Department of Physics, Division of Science & Technology, University of Education, Lahore, Pakistan
[e] Research Center in Industrial Technologies CRTI, P.O. Box 64, 16014 Cheraga, Algiers, Algeria

ARTICLE INFO

Keywords:
Single layer solar cells
Numerical simulations
CGS/CIGS triple-junction solar cell
Silvaco-Atlas Software

ABSTRACT

The simulations have been carried out to study and investigate the performance of the photovoltaic J-V characteristics of triple-junction solar cells based on Cu(In,Ga)Se2 absorbers using 2D Silvaco/Atlas simulator. The triple-junction configuration was considered as a single layer of CGS on top while the CIGS single layer was separated for middle and bottom cells. The investigations for CIGS solar cell presented in this article are in close agreement with the already observed numerical and experimental data. The photovoltaic J-V characteristics for the proposed CGS/CIGS triple-junction solar cell, such as the short-circuit current density, open-circuit voltage, fill factor and power conversion efficiency have been investigated and observed to be 13.49 mA/cm2, 2.64 V, 86.56% and 30.85%, respectively. The proposed configuration offers improved conversion efficiency up to 33.27% at current matching point. The entire inquiry on CIGS solar cells yields a prospective idea for single and triple-junction solar cells with high efficiency.

1. Introduction

The requirement for the cost-effective and highly efficient solar cells to replace the existing silicon-based solar cells is the top priority of the solar industry. In the last decade, many investigations have been reported regarding the development of efficient solar cells [1,2]. Literature suggested that the viability of dual solar cells is possible by adopting a low-cost synthesis methodology with minimal consumption of material [3]. Among various materials, copper indium gallium diselenide (CIGS) is considered to be the most promising material due to its tunable band-gap with a higher absorption coefficient, radiation hardness, high power and outdoor stability [4–7]. Most recently, the reported efficiency for CIGS-based solar cells is 20.3 and 19.9% as recorded by the Centre of Solar Energy and Hydrogen Research (ZSW) [8] and the National Renewable Energy Laboratory (NREL) [9], respectively. Improved efficiency is possible when solar cells are fabricated in layered (multi-junction) configurations for utilizing the maximum fraction of the solar spectrum [10–13]. Triple-junction solar cell configuration consists of a high band-gap window layer at the top, a middle layer and

* Corresponding author. Research Center in Industrial Technologies, P.O. Box 64, Cheraga, 16014, Algiers, Algeria.
E-mail addresses: s.boudour@crti.dz, boudoursamah@gmail.com (S. Boudour).

https://doi.org/10.1016/j.micrna.2024.207812
Received 20 December 2023; Received in revised form 27 February 2024; Accepted 28 February 2024
Available online 29 February 2024

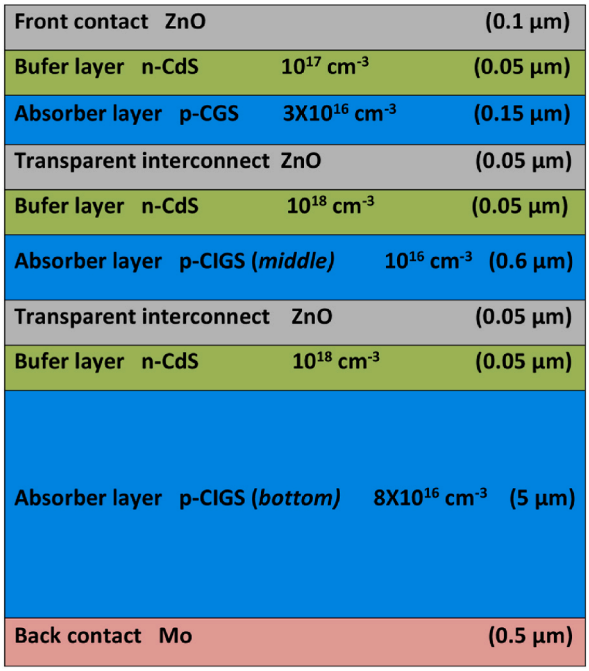

Fig. 1. Design of the simulated CGS/CIGS triple-junction solar cell with sub-cells connected by an interconnect formed of transparent ZnO.

a low band-gap absorbing bottom layer [14]. Theoretical and experimental investigations revealed that nanocrystalline thin films of CGS and CIGS exhibit improved energy band-gaps and have potential applications in the PV industry. Soheili et al. [10,11,13] have reported performance improvement studies of dual-junction solar cells by using several anti-reflector layers. The use of triple-junctions in the fabrication of solar cells has already been reported in many theoretical studies. Faine et al. [15] have reported the investigation of single, dual and triple-junction solar cells by using spectral irradiance models and semi-empirical models. McMahon et al. [16] reported the importance of the material to be used as a top layer in solar cell configuration. There is a consensus among researchers that the provision of better insights is possible when the solar cell configurations are simulated rather than experimental investigations. The best-ever efficiency for a III-V triple-junction solar cell reported so far is 40% [17].

Herein, we report theoretical investigations based on the study of single and triple-junction solar cells using Silvaco-Atlas, a device simulator [18]. Comparison of single and triple-junction CGS/CIGS in terms of their performance is also part of this work.

2. Triple-junction cell structure and numerical simulation

2.1. Structural configuration

For thin film solar cells, light absorption can be maximized by using absorbing layers of different band-gap energy. In the present study, a triple-junction solar cell is configured by using three different cells (top, middle and bottom) with optimum thickness and band-gap energy, as shown in Fig. 1. A thin layer of CGS with a band gap energy of 1.69 eV was used as the top-cell, a layer of normal thickness of CIGS with a band gap energy of 1.36 eV was used as a middle-cell and a slightly thick layer was used as a bottom-cell with a band gap energy of 1.16 eV [19]. All three layers/cells are coupled with a layer of ZnO that acts as a window or transparent conducting oxide layer (TCO) [20]. The proposed design aims to transmit the maximum number of incident photons and is capable to generate sufficient output power. This triple-junction cell was illuminated by a power density of 100 mW/cm^2 under AM1.5 G solar spectrum. The photons are incident normally onto the ZnO layer used as front cathode contact, however, a layer of molybdenum was used as back anode contact. The considered solar cell geometry was simulated with the help of the Silvaco-Atlas 2D simulator by using a drift diffusion transport model.

2.2. Physical model

The Silvaco-Atlas 2D simulator was employed to solve Poisson's equation coupled with the continuity relations for both types of charge carriers i.e., electrons and holes in steady-state. The basic semiconductor equations employed in the simulator have been solved by the Newton method [21].

The basic parameters studied in this work are.

- Energy bang gap (E_g);

Table 1
Material parameters used in the simulation.

Parameter	CdS	CGS/CIGS/CIGS
Band gap energy *Eg* (eV)	2.4	1.69/1.36/1.16
Electron affinity χe (eV)	4.2	4.5
Relative permittivity ε_r (F.cm^{-1})	10	13.6
Density of states at conduction band N_C (cm^{-3})	2.2×10^{18}	2.2×10^{18}
Density of states at valence band N_V (cm^{-3})	1.8×10^{19}	1.8×10^{19}
Electron mobility μn (cm^2/Vs)	100	100
Hole mobility μp (cm^2/Vs)	25	25
Gaussian defect states	**CdS**	**CGS/CIGS/CIGS**
Gaussian defect density N_{GA}, N_{GD} (cm^{-3})	10^{15} (A)	10^{15} (D)
Peak energy position EGA, EGD (eV)	1.2 (A)	0.84/0.68/0.58 (D)
Standard energy deviation W_{GA}, W_{GD} (eV)	0.1 (A)	0.1 (D)
Electron capture cross section σ_n (cm^2)	10^{-15}	$2*10^{-15}$
Hole capture cross section σ_p (cm^2)	10^{-17}	$3*10^{-13}$
Surface recombination velocity for electrons and holes (cm.s^{-1})	S_n	S_p
CdS/CGS interface	10^5	10^5
CdS/CIGS interface	10^5	10^5
CdS/CIGS interface	10^5	10^5
Front contact	10^5	10^5
Back contact	10^5	10^5

- Relative permittivity (ε_r);
- Electron affinity and electron/hole mobilities (χ_e, μ_n, μ_p);
- Effective density of states in the conduction (N_C) and valence (N_V) bands;
- Gaussian defect densities (N_{GA}, N_{GD});
- Peak energy positions (E_{GA}, E_{GD});
- Standard energy deviations (W_{GA}, W_{GD});
- Electron and Hole capture cross-section (σ_n, σ_p);
- Surface recombination velocities for electrons and holes (S_n, S_p);

The input data used to simulate each cell layer by Atlas-Silvaco is given in Table 1 [22–27]. The band gap value for $CuIn_{1-x}Ga_xSe_2$ was estimated using an empirical expression:

$$E_g[eV] = 1.010 + 0.626.x - 0.167.x(1-x), \tag{1}$$

where the value of band gap energy (E_g) was used to vary from 1.01 eV to 1.69 eV for $x = 0$ ($CuInSe_2$) and $x = 1$ ($CuGaSe_2$), respectively [28].

For the top, middle and bottom layers, the value of x is taken as 1, 0.66 and 0.33, respectively. Gaussian distribution was used to model the defect density within the CIGS and CdS layers as:

$$g_{GD}(E) = N_{GD} \exp\left[-\left[\frac{E - E_{GD}}{W_{GD}}\right]^2\right], \tag{2}$$

$$g_{GA}(E) = N_{GA} \exp\left[-\left[\frac{E_{GA} - E}{W_{GA}}\right]^2\right], \tag{3}$$

where, E represents defects energy. The subscripts letters G, A and D represent Gaussian, Acceptor and Donor states, respectively. To formulate the total density of states (DOS), the effective density of states N_{GA} or N_{GD}, peak energy position E_{GA} or E_{GD} and standard energy deviation W_{GA} or W_{GD} are considered [21].

The Shockley-Read-Hall recombination relation was used to access the Gaussian defect distribution in semiconducting layers of solar cells:

$$R_{SRH} = \frac{pn - n_i^2}{\tau_p\left(n + n_i\, exp^{\frac{E_i - E_T}{kT_L}}\right) + \tau_n\left(p + n_i\, exp^{\frac{-(E_i - E_T)}{kT_L}}\right)}, \tag{4}$$

$$\tau_n = \frac{1}{\sigma_n v_{th} N_t} \quad \text{And } \tau_p = \frac{1}{\sigma_p v_{th} N_t}, \tag{5}$$

where, $\boldsymbol{\tau_n}$ and $\boldsymbol{\tau_p}$ represent the lifetime parameter for electrons and holes, respectively. $\boldsymbol{\sigma_n}$ and $\boldsymbol{\sigma_p}$ represent the capture cross-section, $\boldsymbol{\nu_{th}}$

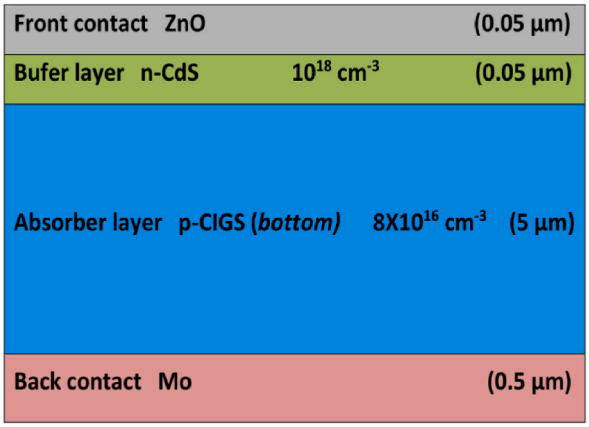

Fig. 2. Single CIGS bottom-cell.

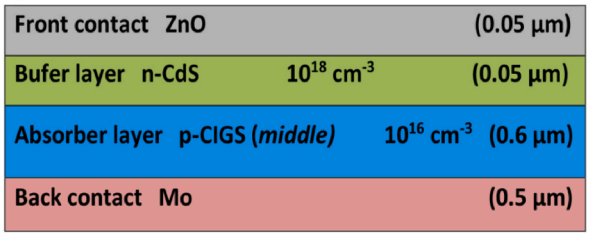

Fig. 3. Single CIGS middle-cell.

represents the thermal velocity, N_t represents the bulk trap density, n_i represent the spatially changing level of intrinsic concentration, E_i represents the intrinsic Fermi level, E_T represents the trap energy level and T_L represents the temperature [29].

It is obvious that there would be a high defect concentration at the interfaces due to lattice mismatching [30] and the surface recombination can be expressed as:

$$R_{Surf} = \frac{pn - n_i^2}{\tau_p^{eff}\left(n + n_i\, exp^{\frac{E_i - E_T}{kT_L}}\right) + \tau_n^{eff}\left(p + n_i\, exp^{\frac{-(E_i - E_T)}{kT_L}}\right)}, \tag{6}$$

$$\frac{1}{\tau_n^{eff}} = \frac{1}{\tau_n^i} + \frac{d_i}{A_i} S.N \quad \text{And} \quad \frac{1}{\tau_p^{eff}} = \frac{1}{\tau_p^i} + \frac{d_i}{A_i} S.P, \tag{7}$$

where, $\boldsymbol{\tau}_{ni}$ and $\boldsymbol{\tau}_{pi}$ are the bulk lifetime calculated at node i along the interface and which may be a function of the impurity concentration as well. The S, N, and P Parameters are the recombination velocities for electrons and holes, respectively [21].

The optical parameters like refractive index and extinction coefficient were taken from the literature [31–38] and are used to study the characteristics of triple-junction solar cells. The optical parameters for metal contacts are obtained from the Sopra database. The overall simulations for the proposed configuration are carried out at 300 K.

3. Results and discussions

3.1. Modeling of single CGS and CIGS solar cells

Table 1 depicted all the input parameters used to simulate CGS and CIGS solar cells. A single CIGS bottom layer consists of a heap of layers with an active area of 1 cm^2. The multilayers from bottom to top are as follows: the back metal contacts are of Mo (0.5 µm), the p-doped CIGS (4.3 µm) with $x = 0.33$ ($E_g = 1.16$ eV) used as an absorber layer, the n-doped CdS layer (0.05 µm) and ZnO layer (0.1 µm) as buffer and window layers, respectively. The geometrical dimensions of the single CIGS bottom-cell are similar to the cell parameters as available in the literature and are shown in Fig. 2 [34]. The Ga composition was varied from $x = 0.33$ to 0.66 and 1 corresponding to the energy band gap values as 1.16, 1.36 and 1.69 eV, respectively. The doping concentration of the CGS, CIGS and CdS has been chosen after optimization to enhance the conversion efficiency of layers.

The top and middle cells follow the same structure as the previous bottom-cell, but with different layer characteristics. Specifically, the middle-cell of the CIGS solar panel consists of a p-type CIGS absorber, n-type CdS buffer, TCO layer made of ZnO material on top,

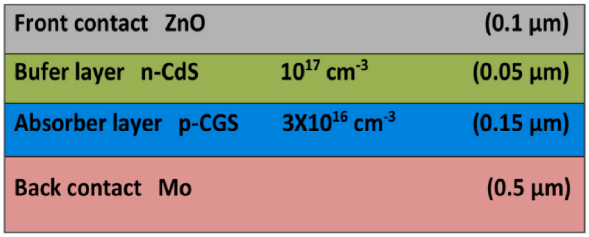

Fig. 4. Single CIGS top-cell.

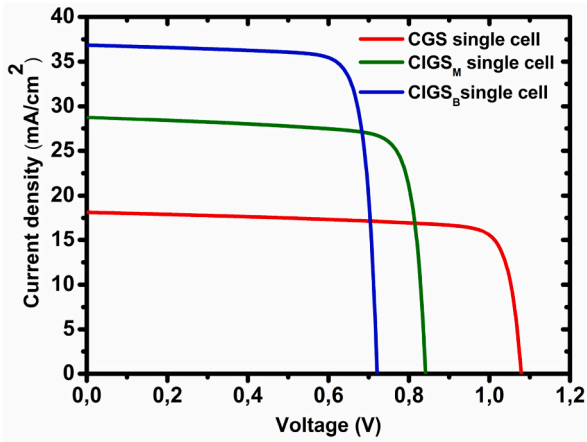

Fig. 5. J–V characteristics for $CIGS_B$ single cell, $CIGS_M$ single cell, CGS single cell and CGS/CIGS triple-junction solar cell.

Table 2
Photovoltaic parameters for the bottom, middle, top and triple-junction cells.

	Jsc (mA/cm^2)	*Voc* (V)	*FF* (%)	*η* (%)
CGS single cell	18.13	1.08	80.35	15.79
CGS top-cell	17.58	1.08	80.79	15.41
CIGS single cell	28.75	0.84	81.03	19.71
CIGS middle-cell	16.26	0.83	78.20	10.58
CIGS bottom-cell	13.36	0.71	82.17	07.69
CGS/CIGS triple-junction cell	13.49	2.64	86.56	**30.85**

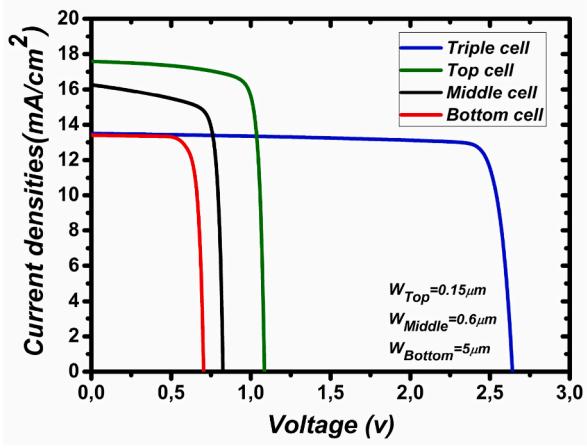

Fig. 6. J–V characteristics for CIGS bottom-cell, CIGS middle-cell, CGS top-cell and CGS/CIGS triple-junction solar cells.

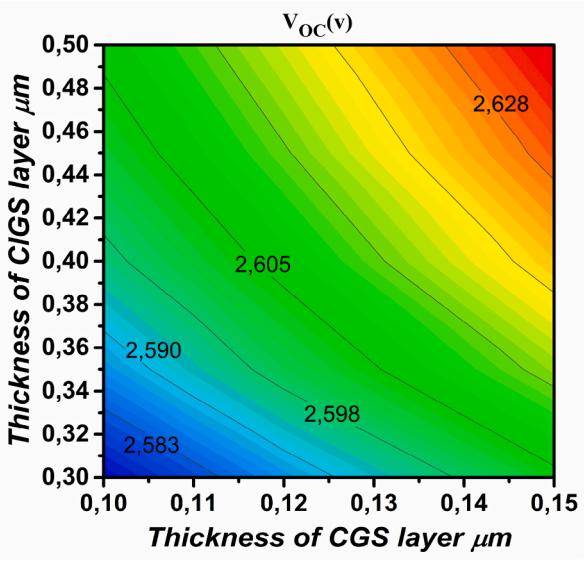

Fig. 7. Contour plot for the variation of V_{oc} as a function of the thicknesses of CGS and CIGS layers.

and a Mo layer as the back contact. This structure is shown in Fig. 3, with Ga composition $x = 0.66$ and an energy band-gap of 1.36 eV.

On the other hand, the top-cell is a CGS solar cell comprises a p-type CGS absorber, n-type CdS buffer, TCO layer made of ZnO material on top and a Mo layer as a back contact, with Ga composition $x = 1$ and an energy band-gap of 1.69 eV. Fig. 4 displays the configuration of CGS top-cell.

Fig. 5 shows the J-V characteristics for the individual CGS and CIGS solar cells. To verify the accuracy of our model, we compared the performance parameters of the CIGS bottom-cell with those reported in the literature and the findings are presented in Table 2.

3.2. Modeling of CGS/CIGS triple-junction solar cell

Fig. 6 displays the J-V characteristics for 4 types of cells: CGS top-cell, CIGS middle-cell, CIGS bottom-cell and CIGS/CIGS triple-junction solar cell, Table 2 provides a summary of the electrical parameters for four different cells: CIGS top-cell, CIGS middle-cell, CIGS bottom-cell, and CGS/CIGS triple-junction cell. To generate the J-V curves of the top-cell, the middle-cell and bottom-cell, the contacts for the anode and cathode of the top-cell were placed on the interconnect ZnO layer and the front ZnO layer, respectively. Similarly, for the bottom-cell, the anode and cathode contacts were positioned on the back Mo layer and the interconnect ZnO layer, respectively.

It has been observed that the open-circuit voltage of CGS/CIGS triple-junction cell is found to be 2.64 V and is equivalent to the sum of open circuit voltage for the top, middle and bottom cells i.e., 1.08, 0.83 and 0.71 V, respectively. It is important to mention that, the proposed triple-junction geometry of solar cells composed of CGS and CIGS cells is the correct model. This claim is validated by the J_{sc} calculations for the triple-junction cell (13.35 mA/cm^2) which is observed to be limited by a small current at the CIGS bottom-cell with $J_{sc} = 13.17$ mA/cm^2. This observation regarding the non-ideal matching of current between the top, middle and bottom layers suggested the need for the completely optimized bottom and top layers. Moreover, the fill factor *FF* for the triple-junction is observed to be 86.56% with an efficiency of 30.85% which is better than *FF* for the top-cell (80.79%) with an efficiency of 22.01%, for the middle-cell (78.2%) with an efficiency of 19.71% and the bottom-cell (82.17%) with an efficiency of 15.79%. It is noteworthy that simulations for this triple junction cell have not been previously reported.

Upon comparing the results of the CIGS single cell with the CIGS bottom-cell in the CGS/CIGS triple-junction solar cell, a significant decrease in the photovoltaic parameters of the CIGS bottom-cell can be observed. This degradation can be attributed to the top layers absorbing a portion of the incident light.

3.3. Optimization of photovoltaic cell parameters

By reducing the thickness of the top and middle cells in the triple-junction solar cell, the distribution of light between the three sub-cells can be altered, resulting in an increase in the current of the bottom-cell at the expense of the top and middle cells. However, for optimal efficiency, the short-circuit current density of the bottom-cell (J_{scb}) must be lower than that of the top-cell (J_{sct}) and middle-cell (J_{scm}). In such cases, reducing the thickness of the middle and top cells can achieve current matching, where $J_{scb} = J_{scm} = J_{sct} = J_{sc}$. This ensures that the triple-junction cell current density is limited by the lowest of J_{scb}, J_{scm} and J_{sct}. The cell efficiency is optimized by reducing the thickness of the top and middle cells to achieve current matching.

To improve the performance of the CGS/CIGS triple-junction solar cell, we conducted calculations that involved adjusting the

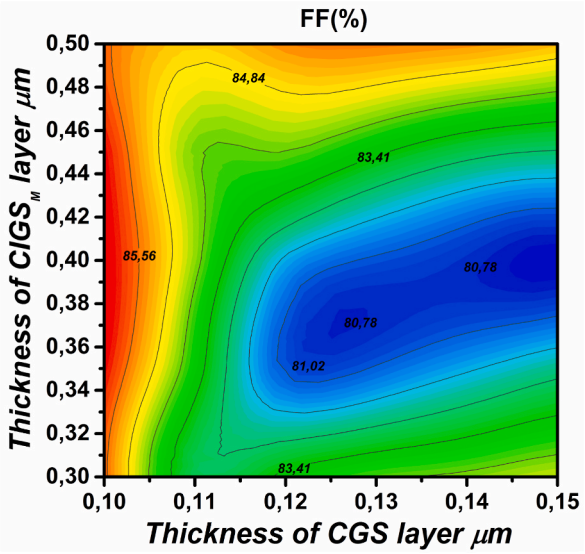

Fig. 8. Contour plot of the FF as a function of the thicknesses of the CGS and CIGS layers.

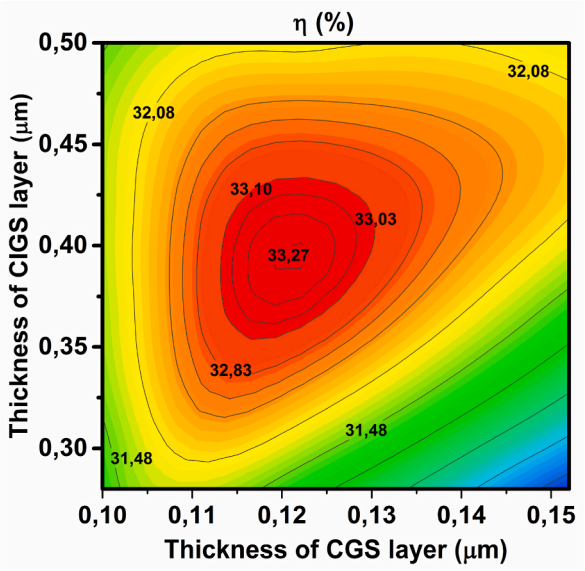

Fig. 9. Short-circuit current density of CGS/CIGS triple-junction solar cell vary as a function of the CGS and CIGS layer thicknesses in CGS top and CIGS middle cells.

thickness of the CGS layer in the top-cell from 0.1 μm to 0.15 μm, while simultaneously varying the thickness of the CIGS layer in the middle-cell from 0.3 μm to 0.5 μm. While maintaining a constant thickness of 5 μm for the CIGS layer of bottom-cell, the optimal range of thickness for the best performance was identified through the cell's structure, as illustrated in Fig. 1.

Fig. 7 illustrates how the open-circuit voltage (V_{oc}) of the triple-junction cell is affected by changes in the thicknesses of the CGS and CIGS layers. Across the entire range of thicknesses, an increase in both CGS and CIGS thicknesses leads to an increase in the open-circuit voltage. It is worth noting that the minimum voltage is 2.57 V at the lowest pair of thicknesses (0.12 μm for CGS and 0.3 μm for CIGS), while the maximum voltage is 2.63 V at the highest pair of thicknesses (0.15 μm for CGS and 0.5 μm for CIGS). This indicates that both the CGS and CIGS thicknesses have a same impact on the V_{oc} of CGS/CIGS triple-junction cell. Additionally, the open-circuit voltage of the triple-junction cell in all cases is simply the sum of the open circuit voltages of the top, middle, and bottom cells. The variation of the fill factor of a triple-junction solar cell with changes in the thicknesses of CGS and CIGS layers can be observed in the graph presented in Fig. 8. When the thicknesses of CGS and CIGS layers are set at 0.12 and 0.4, respectively, the fill factor of the triple-junction solar cell drops to a minimum value of 78%–81%. It's worth mentioning that the fill factor is directly affected by any changes made to the CIGS layer thickness in the middle cell.

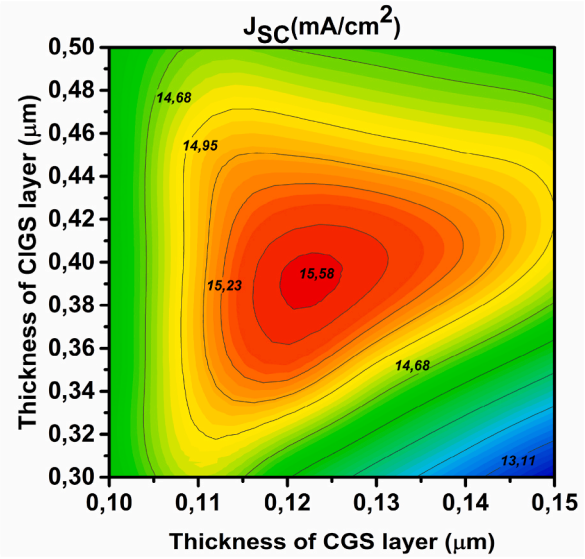

Fig. 10. Conversion efficiency of CGS/CIGS triple-junction solar cell varies with the CGS and CIGS layer thicknesses in CGS top-cell and CIGS middle-cell.

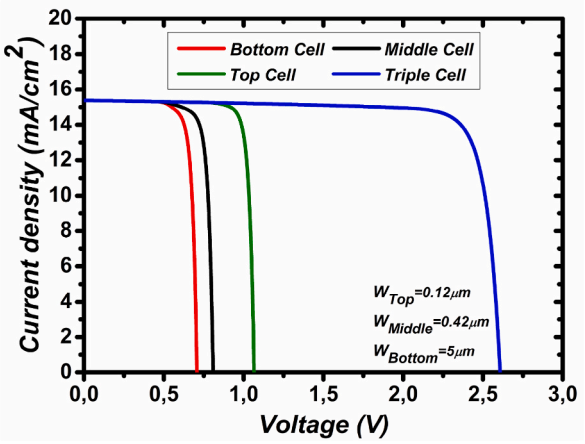

Fig. 11. J–V characteristics of CGS top-cell, CIGS middle-cell, CIGS bottom-cell and CGS/CIGS triple junction solar cell under current matching point.

Table 3
Photovoltaic parameters of top, middle, bottom and triple-junction solar cells were optimized under the current matching point.

	Jsc (mA/cm^2)	*Voc* (V)	*FF* (%)	*η* (%)
CGS top-cell	15.58	1.07	84.21	14.14
CIGS middle-cell	15.58	0.82	78.72	10.07
CIGS bottom-cell	15.58	0.71	82.34	09.06
CGS/CIGS triple-junction cell	15.58	2.60	84.13	**33.27**

Fig. 9 illustrates the relationship between the thickness of the top-cell and middle-cell and the resulting short-circuit current density J_{sc}. The data suggests that a thickness of 0.12 μm for CGS layer and 0.4 μm for CIGS layer achieves the optimal J_{sc} as a current matching point, resulting an optimal value of J_{sc} at about 15.58 mA/cm^2.

Fig. 10 showcases contour plots that display the correlation between changes in the thickness of CGS and CIGS layers and the energy conversion efficiency. It's clear that the thicknesses of the CGS and CIGS layers correspond to the point (0.12 μm, 0.4 μm) where the highest efficiency level of about 33.27% is achieved. The top, middle, and bottom cells reach an optimal current exactly in current matching point. Fig. 11 illustrates the J-V curves, which exhibit the electrical properties of the recommended solar cell design at the

Table 4
J-V characteristics of proposed triple-junction solar cell in comparison with previous works.

Solar cell configuration	J_{sc} (mA/cm^2)	V_{oc} (V)	FF (%)	η (%)
CIGS single-junction, by Boudour et al. [7]	35.89	0.88	79.77	25.22
CGS/CIGS dual-junction, by Abdolmaleky et al. [6]	27.09	1.9	86.21	44.37
CGS/CIGS dual-junction, by Soheili et al. [10]	25.57	2.03	87.14	45.23
GaInP/GaAs dual-junction, by Bakour et al. [12]	13.66	2.51	89.91	30.82
CGS/CIGS dual-junction, by Soheili et al. [13]	25.17	2.14	86.88	46.80
CIGS/CIGS dual-junction, by Bouanani et al. [34]	18.82	1.84	82.54	27.03
InGaP/GaAs/InGaAs triple-junction, by Rashmi et al. [39]	33.4	1.27	99.5	30.91
CGS/CIGS triple-junction, this work	15.58	2.60	84.13	**33.27**

ideal thicknesses of the top and middle layers, approximately 0.12 and 0.4 μm, respectively. As a result, Table 3 summarizes the photovoltaic properties of the herein designed solar cell at the current matching point. While, using photovoltaic J-V characteristics, Table 4 summarizes a comparison between the reported herein triple-junction solar cell with some recent reported single, dual and triple-junction solar cells.

The results listed in Table 4 indicated that the majority of dual-junction had the best conversion efficiencies, even reaching 47.737% by adding an aluminium back mirror layer at the bottom surface of solar cell as reported by Soheili et al. [13]. Compared to the CIGS single-junction in addition to the triple-junction with different materials, the CGS/CIGS triple-junction had the most highly efficiency of 33.27 %. While, the best open-circuit voltage was achieved by the CGS/CIGS triple-junction solar cell reported herein this work. As a perspective, the addition of anti-reflector coating layers and back mirror layer [13] may improve the overall performance of CGS/CIGS triple-junction solar cell.

4. Conclusion

In summary, the electrical characteristics of CGS/CIGS single and triple-junction solar cells have been investigated by using Silvaco/Atlas (2D) numerical simulator under AM1.5 illuminations. Improved conversion efficiency up to 30.85% has been observed for the CGS/CIGS triple-junction solar cell which is far better than the single layers of CGS and CIGS solar cells. The obtained results reveal that the thickness of top and middle layers plays an important role in maximizing the overall efficiency of the solar cell. The proposed triple-junction solar cell depicts an improved conversion efficiency of 33.27% specifically for the thickness of CGS and CIGS layers as 0.12 and 0.4 μm, respectively. The obtained geometry of CGS/CIGS triple-junction solar cell structure would have the potential to be fabricated experimentally for advancements in the solar cell industry.

CRediT authorship contribution statement

Rafik Zouache: Writing – review & editing, Writing – original draft, Visualization, Validation, Software, Methodology, Investigation, Conceptualization. **Idris Bouchama:** Writing – review & editing, Supervision, Methodology, Conceptualization. **Okba Saidani:** Visualization, Validation, Methodology, Investigation, Data curation, Conceptualization. **Mohamed Amine Ghebouli:** Writing – review & editing, Visualization, Validation. **M. Saeed Akhtar:** Writing – review & editing. **M.A. Saeed:** Writing – review & editing. **Samah Boudour:** Investigation, Conceptualization, Writing – review & editing. **Leila Lamiri:** Writing – review & editing. **Ouafia Belgherbi:** Writing – review & editing.

Declaration of competing interest

The authors declare that they have no known competing financial interests or personal relationships that could have appeared to influence the work reported in this paper.

Data availability

No data was used for the research described in the article.

Acknowledgments

The authors would like to acknowledge Silvaco Inc. for the Silvaco/Atlas Simulation tool.

References

[1] T.P. Dhakal, C.Y. Peng, R.R. Tobias, R. Dasharathy, C.R. Westgate, Characterization of a CZTS thin film solar cell grown by sputtering method, Sol. Energy 100 (2014) 23–30.
[2] T.D. Lee, A.U. Ebong, A review of thin film solar cell technologies and challenges, Renew. Sustain. Energy Rev. 70 (2017) 1286–1297.
[3] Y. Wei, D. Zhuang, M. Zhao, N. Zhang, X. Yu, R. Sun, L. Zhang, X. Lyu, X. Peng, J. Wei, Fabrication of wide band-gap CuGaSe2 solar cells for tandem device applications by sputtering from a ternary target and post selenization treatment, Mater. Lett. 230 (2018) 128–131.

[4] C.H. Huang, Effects of Ga content on Cu(In,Ga)Se2 solar cells studied by numerical modeling, J. Phys. Chem. Solid. 69 (2008) 330–334.
[5] S. Tobbeche, S. Kalache, M. Elbar, M.N. Kateb, M.R. Serdouk, Improvement of the CIGS solar cell performance: structure based on a ZnS buffer layer, Opt. Quant. Electron. 51 (2019) 1–13.
[6] M. Abdolmaleky, F. Shama, Design of an efficient double-junction CGS/CIGS solar cell, Optik 172 (2018) 271–277.
[7] S. Boudour, I. Bouchama, S. Laidoudi, W. Bedjaoui, L. Lamiri, O. Belgherbi, S. Aziez, Study of CIGS pseudo-homojunction thin film solar cell using SCAPS-1D, East European Journal of Physics (4) (2022) 145–152.
[8] M. Elbar, S. Tobbeche, A. Merazga, Effect of top-cell CGS thickness on the performance of CGS/CIGS tandem solar cell, Sol. Energy 122 (2015) 104–112.
[9] H. Zhang, B. Niesen, E. Hack, S. Jenatsch, L. Wang, A.C. Véron, F. Nüesch, Cyanine tandem and triple-junction solar cells, Org. Electron. 30 (2016) 191–199.
[10] A. Soheili, M. Hayati, F. Shama, An optimized efficient double junction CGS/CIGS solar cell with improved performance, Optik - International Journal for Light and Electron Optics 222 (2020) 165461.
[11] A. Soheili, M. Hayati, F. Shama, A double junction CZTS/CIGS solar cell optimization using analytical method, Micro and Nanostructures 166 (2022) 207215.
[12] A. Bakour, A. Saadoune, I. Bouchama, F. Dhiabi, S. Boudour, M.A. Saeed, Effect and optimization of ZnO layer on the performance of GaInP/GaAs tandem solar cell, Micro and Nanostructures 168 (2022) 207294.
[13] A. Soheili, M. Hayati, F. Shama, Conversion efficiency improvement of CGS/CIGS photovoltaic cell, Optik 287 (2023) 171089.
[14] S.P. Philipps, G. Peharz, R. Hoheisel, T. Hornung, N.M. Al-Abbadi, F. Dimroth, A.W. Bett, Energy harvesting efficiency of III–V triple-junction concentrator solar cells under realistic spectral conditions, Sol. Energy Mater. Sol. Cell. 94 (2010) 869–877.
[15] P. Faine, S.R. Kurtz, C. Riordan, J.M. Olson, The influence of spectral solar irradiance variations on the performance of selected single-junction and multijunction solar cells, Sol. Cell. 31 (1991) 259–278.
[16] W.E. McMahon, K.E. Emery, D.J. Friedman, L. Ottoson, M.S. Young, U.S. Ward, C.M. Kramer, A. Duda, S. Kurtz, An on-sun comparison of GaInP2/GaAs tandem cells with top cell thickness varied, in: Proceedings of the 31st, IEEE Photovoltaic Specialists Conference, Orlando, FL, USA, 2005 715718.
[17] W. Guter, J. Schone, S.P. Philipps, M. Steiner, G. Siefer, A. Wekkeli, E. Welser, E. Oliva, A.W. Bett, F. Dimroth, Current-matched triple-junction solar cell reaching 40.1% conversion efficiency under concentrated sunlight, Appl. Phys. Lett. 94 (2009) 223504, 1–223504-3.
[18] ATLAS Device Simulation Software, SILVACO International. Santa Clara, CA, 2018.
[19] P. Jackson, D. Hariskos, E. Lotter, S. Paetel, R. Wuerz, R. Menner, W. Wischmann, M. Powalla, New world record efficiency for Cu(In,Ga)Se2 thin-film solar cells beyond 20, Prog. Photovoltaics Res. Appl. 19 (2011) 894–897.
[20] M. Elbar, S. Tobbeche, Numerical simulation of CGS/CIGS single and tandem thin-film solar cells using the silvaco-atlas software, Energy Proc. 74 (2015) 1220–1227.
[21] User manual of Silvaco ATLAS software, version 5.18.3. R, 2012.
[22] M. Gloeckler, J.R. Sites, W.K. Metzger, Grain-boundary recombination in Cu(In,Ga)Se2 solar cells, J. Appl. Phys. 98 (11) (2005) 113704.
[23] A. Cherouana, R. Labbani, Numerical simulation of CZTS solar cell with silicon back surface field, Mater. Today Proc. 5 (5) (2018) 13795–13799.
[24] H. Heriche, Z. Rouabah, N. Bouarissa, New ultra-thin CIGS structure solar cells using SCAPS simulation program, Int. J. Hydrogen Energy 42 (15) (2017) 9524–9532.
[25] S. Benabbas, Z. Rouabah, N. Bouarissa, N. Chelali, The role of back surface field SnS layer in improvement of efficiency of CdTe thin film solar cells, International Journal for Light and Electron Optics 127 (15) (2016) 6210–6217.
[26] M.W. Bouabdelli, F. Rogti, M. Maache, A. Rabehi, Performance enhancement of CIGS thin-film solar cell, International Journal for Light and Electron. Optics 216 (2020) 164948.
[27] S.R.I. Biplab, M.H. Ali, M.M.A. Moon, M.F. Pervez, M.F. Rahman, J. Hossain, Performance enhancement of CIGS-based solar cells by incorporating an ultrathin BaSi2 BSF layer, J. Comput. Electron. 19 (1) (2019) 342–352.
[28] R. Zouache, I. Bouchama, O. Saidani, Numerical study of high-efficiency CIGS solar cells by inserting a BSF μc-Si:H layer, J. Comput. Electron. 21 (2022) 1386–1395.
[29] J. Raymond, Five-junction Solar Cell Optimization Using Silvaco-Atlas, Thesis, Naval postgraduate school, Monterey, California, 2017.
[30] J.M. Olson, D.J. Friedman, S. Kurtz, Handbook of Photovoltaic Science and Engineering, first ed., John Wiley and Sons, West Sussex, 2003.
[31] P.D. Paulson, R.W. Birkmire, W.N. Shafarman, Optical characterization of CuIn1-xGaxSe2 alloy thin films by spectroscopic ellipsometry, J. Appl. Phys. 94 (2003) 879–888.
[32] E.D. Palik, Handbook of Optical Constants of Solids III, Boston Academic press, San Diego, London, 1998.
[33] M. Richter, C. Schubbert, P. Eraerds, I. Riedel, J. Keller, J. Parisi, T. Dalibor, A. Avellán-Hampe, Optical characterization and modeling of Cu(In,Ga)(Se,S)2 solar cells with spectroscopic ellipsometry and coherent numerical simulation, Thin Solid Films 535 (2013) 331–335.
[34] B. Bouanani, A. Joti, F.S. Bachir Bouiadjra, A. Kadid, Band gap and thickness optimization for improvement of CIGS/CIGS tandem solar cells using silvaco software, Optik 204 (2020) 164217.
[35] K. Ramanathan, M.A. Contreras, C.L. Perkins, S. Asher, F.S. Hasoon, J. Keane, D. Young, M. Romero, W. Metzger, R. Noufi, J. Ward, A. Duda, Properties of 19.2% efficiency ZnO/CdS/CuInGaSe2 thin-film solar cells, Prog. Photovoltaics Res. Appl. 11 (4) (2003) 225–230.
[36] I. Repins, M. Contreras, M. Romero, Y. Yan, W. Metzger, J. Li, R. Noufi, Characterization of 19.9%-efficient CIGS Absorbers, 33rd IEEE Photovoltaic Specialists Conference, 2008, pp. 1–6.
[37] P. Chelvanathan, M.I. Hossain, N. Amin, Performance analysis of copper-indium-gallium-diselenide (CIGS) solar cells with various buffer layers by SCAPS, Curr. Appl. Phys. 10 (2010) S387–S391.
[38] M. Fathi, M. Abderrezek, F. Djahli, M. Ayad, Study of thin film solar cells in high temperature condition, Energy Proc. 74 (2015) 1410–1417.
[39] C. Rashmi, S. Poonam, G.A. Kumar, Design and analysis of multi junction solar photovoltaic cell with graphene as an intermediate layer, J. Nanosci. Nanotechnol. 20 (6) (2020) 3693–3702.